Large-Scale Characteristics and Probability of Rapidly Intensifying Tropical Cyclones in the Western North Pacific Basin

SHOUJUAN SHU AND JIE MING

Key Laboratory of Mesoscale Severe Weather, Ministry of Education, and School of Atmospheric Sciences, Nanjing University, Nanjing, China

PENG CHI

Jiangxi Air Traffic Management Sub-bureau, Civil Aviation Administration of China, Nanchang, China

(Manuscript received 11 April 2011, in final form 20 October 2011)

ABSTRACT

The China Meteorological Administration (CMA) and the National Centers for Environmental Prediction (NCEP) reanalysis datasets are employed to examine the large-scale characteristics of rapidly intensifying western North Pacific tropical cyclones (TCs). The results show that of all 27 581 samples for the period 1970–2007, 85%, 65%, and 47% of all tropical depressions (TDs), tropical storms (TSs), and typhoons (TYs), respectively, intensify. Of the 1214 TCs, 18%, 70%, 30%, and 10% of all tropical cyclones, supertyphoons, severe typhoons, and typhoons, respectively, underwent rapid intensification (RI) at least once during their lifetime. Three kinds of cases—RI, slow change in intensity (SC), and rapid decay (RD)—during the period 1982–2007 are used to analyze the large-scale conditions associated with them. The comparison shows that the RI cases tend to occur farther south and east than the non-RI cases. In addition, the RI cases have a more westerly component of motion and intensify more during the preceding 12 h than do the non-RI cases. For the non-RI cases, the SC cases tend to have a lower initial intensity and a lower speed of motion than do the RD cases. Also, the RI cases are farther from their maximum potential intensity and develop in warmer water, lower vertical shear, and more easterly upper-tropospheric flow than do the non-RI cases. The probability of RI for TCs is estimated by using the rapid intensify index (RII) developed in this study for the western North Pacific basin. The verification based upon the cross validation shows that the RII is skillful relative to climatology.

1. Introduction

While some improvements have been made in operational tropical cyclone (TC) intensity forecasting in recent years (DeMaria et al. 2007), the forecasting of intensity changes in TCs has strikingly large errors especially during TC rapid intensification (RI) (Elsberry et al. 2007). This is, in part, attributed to our limited understanding of the physical mechanisms that are responsible for these rare events.

In the past, researchers have typically examined the role that the ocean, inner-core processes, and environmental interactions play in TC intensity changes. Although some intensity change studies have examined the importance of all three of these effects, most have focused on only one of these three areas. The results of some more notable TC intensity change studies, as well as some that were described in the more recent literature, are discussed below with emphasis placed on their relevance to RI.

The ocean has long been recognized as having a fundamental impact on TC intensity (Byers 1944; Miller 1958; Malkus and Riehl 1960). Palmén (1948) found that TCs in the Northern Hemisphere formed over oceans with sea surface temperatures (SSTs) higher than 26°–27°C. Chan et al. (2001) have also shown that a critical SST of about 27°C is necessary for a TC to intensify. Intensification proceeds most rapidly when SST is between 27° and 30°C but slows down as SST increases above 30°C. One recent observational study conducted by Shay et al. (2000) showed that Hurricane Opal in 1995 intensified rapidly as it passed over a warm-core eddy in the Gulf of Mexico. Lowag et al. (2008) also found that

Corresponding author address: Shoujuan Shu, Key Laboratory of Mesoscale Severe Weather, Ministry of Education, School of Atmospheric Sciences, Nanjing University, Nanjing 210093, China.
E-mail: sjshu@nju.edu.cn

DOI: 10.1175/WAF-D-11-00042.1

the rapid intensification of Hurricane Bret in 1999 was linked to its passage over a warm ocean eddy and high SST. Though most studies focus solely on the beneficial aspects of the ocean on TC intensity, recent observational (Black 1983) and modeling studies (Sutyrin and Khain 1979; Bender and Ginis 2000) have shown that upwelling and vertical mixing of the cool underlying ocean by the TC vortex can produce a negative feedback between the atmosphere and ocean. However, the studies conducted by Shay et al. (2000) and Hong et al. (2000) suggested that the net effect of the warm eddies was to lessen the magnitude of the cooling of the SST below the TC, thereby decreasing the magnitude of the negative feedback. This finding is consistent with the results of Cione and Uhlhorn (2003), who showed that systems intensified at greater rates when the underlying ocean cooled less. Thus, the primary impact of ocean eddies and other regions of high ocean heat content may be the reduction of the storm-induced negative feedback, as noted by Mainelli et al. (2008).

The importance of inner-core processes on TC intensity change has been examined by many researchers. As noted in Willoughby et al. (1982), marked increases in TC intensity sometimes occur when an outer eyewall contracts and replaces the inner eyewall. Theoretical and modeling results (Montgomery and Kallenbach 1997; Kossin and Schubert 2001) suggest that favorable localized positive potential vorticity or mesovortices within the inner-core region may lead to significant TC intensification. Eastin et al. (2005a,b) suggest that the degree to which the eyewall mesovortices are able to mix high equivalent potential temperature air from the eye into the eyewall may play a key role in determining whether RI actually occurs. Most recent research (Sitkowski and Barnes 2009) showed that a ''spiraling in'' of the eyewall might have initiated the RI for Hurricane Guillermo in 1997.

The importance of large-scale environmental forcing on TC intensity change has been stressed by a number of researchers. Many studies have shown that vertical wind shear plays an important role in modulating TC intensity. Gray (1968) showed that storm development is associated with low vertical wind shear, while Merrill (1988) showed that intensifying TCs tended to have lower vertical shear than nonintensifying ones. As the second-most important predictor, the importance of vertical shear has been tested and proven in the Statistical Hurricane Intensity Prediction Scheme (SHIPS) model (DeMaria and Kaplan 1996). More recently, modeling results conducted by Frank and Ritchie (1999, 2001) have indicated that low shear can result in RI of the TC vortex. In addition to the vertical wind shear, the external forcing from upper-level troughs can also play an important role in TC intensity change (Pfeffer 1958; Pfeffer and Challa 1981). A study performed by Molinari and Vollaro (1990) showed that the interaction with an upper-level trough might have resulted in the rapid deepening of Hurricane Elena in 1985. However, the observational results of Hanley et al. (2001) found that RI is more likely to occur when there is no interaction between a TC and an upper-level system. The modeling results of Frank and Ritchie (1999) and Emanuel (2000) also indicate that RI can occur without external forcing from upper-level troughs or cold lows. These results suggest that external forcing from troughs is not necessary for the occurrence of RI and is likely a factor in the minority of the RI cases.

In addition to the above studies, a few others have focused more explicitly on RI. Bosart et al. (2000) examined an RI episode that occurred during Opal (1995) and concluded that a combination of the environmental forcing and the ocean impacts results in Opal's RI. To better understand and ultimately predict RI, Kaplan and DeMaria (2003, hereafter KD03) examined the large-scale environmental conditions that were conductive for Atlantic basin systems to undergo RI. They found that RIs are embedded in the regions with the following characteristics: weaker vertical wind shear; favorable upper-level forcing from troughs or cold low, warmer SSTs; and higher lower-troposphere relative humidity. Their findings were subsequently used to develop a simple five-predictor RI index (RII) for estimating the probability of RI over the next 24 h. Most recently, Kaplan et al. (2010) developed a revised RII for the Atlantic and eastern North Pacific basins based on their previous works. They found that the relative importance of the individual RI predictors is shown to differ between the two basins, suggesting that the large-scale environmental impact factors are different in different basins and that the RI forecasting model in one basin cannot be applied in another.

In contrast, research focusing on RI for the most active TC basin (the western North Pacific basin) is very limited. Holliday and Thompson (1979) examined the climatological features of RI based on 79 cases during the period 1956–76 over the western North Pacific. The researchers suggested that TC development over warm oceans with SSTs not lower than 28°C is a necessary feature but not a prerequisite for RI. These early results were based on a study of a limited number of samples before 1976, when it is believed that TC intensity data were less reliable. More recently, Ventham and Wang (2007) indicated the environmental characteristics for the very rapid intensification on a synoptic time scale. Wang and Zhou (2008) examined the climatic variability of the RI on seasonal, intraseasonal, interannual, and interdecadal time scales and explored how and to what extent the low-frequency variations of the large-scale

TABLE 1. The definitions of the climatological and persistence, as well as synoptic, variables. The unit for each variable is also shown.

Variable	Unit	Definition
VMX	$m\ s^{-1}$	Maximum sustained surface wind speed
LAT	°N	Latitude
LON	°E	Longitude
SPD	$m\ s^{-1}$	Storm speed of motion
DVMX	$m\ s^{-1}$	Intensity change during the previous 12 h
USTM	$m\ s^{-1}$	u component of storm motion
SST	°C	Sea surface temperature
POT	$m\ s^{-1}$	Maximum potential intensity (MPI) − VMX
SHR	$m\ s^{-1}$	850–200-hPa vertical shear averaged from $r = 200$ to 800 km
U200	$m\ s^{-1}$	200-hPa u component of wind averaged from $r = 200$ to 800 km
T200	°C	200-hPa temperature averaged from $r = 200$ to 800 km
RHLO	%	850–700-hPa relative humidity averaged from $r = 200$ to 800 km
Z850	$10^{-7}\ s^{-1}$	850-hPa relative vorticity averaged for $r \leq 1000$ km
REFC	$m\ s^{-1}\ day^{-1}$	200-hPa relative eddy angular momentum flux convergence averaged from $r = 200$ to 800 km

environment impacted the frequencies and locations of TC RI. A most recent study presented by Yuan and Jiang (2010) showed that relative to the internal process, the large-scale environment played a more important role for the RI of TCs in the western North Pacific. They estimated the probability of RI for TCs in the western North Pacific with the same method used in KD03. But as noted in KD03, the weakness of taking no account of the degree to which conditions were either favorable or unfavorable existed in the original method. Kaplan et al. (2010) therefore developed their RII based on the original version.

One of the greatest challenges in tropical weather forecasting involves the RI of TCs. Unfortunately, little research have been undertaken to study RI, including the reliable large-scale features and the probability forecasting of RI for TCs in the western North Pacific. There is no doubt that a system undergoing RI but without an accurate forecast can produce huge economic losses and claim many lives, especially during its landfall. But for TCs with strong intensity, it is difficult for a forecaster to decide the most accurate time for lifting the typhoon alert. If a TC that is going to make a landfall is forecast to slowly intensify or slowly weaken while it actually undergoes rapid decay (RD) over the succeeding landfalling period, huge indirect economic losses could also be caused due to the disruption of coastal lives. Therefore, accurate RD forecasting is also important from societal and economic points of view. The first goal of this study is to determine if the RI mechanisms proposed in previous studies can be confirmed for a large dataset over the western North Pacific. Another goal of this study is to distinguish environmental conditions that are favorable for RI or RD from conditions that are favorable for cases with slow changes (SC) in intensity, including the slow intensification (SI) cases and the SD cases. In addition, the probability of RI should also be examined in the western North Pacific since the RII metric was developed exclusively for the Atlantic and eastern North Pacific basins.

Section 2 describes the dataset used in the present study. A statistical analysis of the western North Pacific basin's 24-h intensity changes is provided in section 3. A comparison of the conditions present at the start of period of RI to those existing at the start of periods of SC and RD is presented in section 4. The derivation of an RII for the western North Pacific basin and its verification are presented in sections 5 and 6, respectively. Finally, some concluding remarks are offered in section 7.

2. Data and analysis

The database for this study consists of all western North Pacific basin TCs (including nondeveloping depressions) that developed from 1970 to 2007. Table 1 shows the climatological and persistence, as well as synoptic, variables that are evaluated for each TC. These variables were determined from the China Meteorological Administration (CMA) best-track dataset (CMA BTDAT) and the U.S. daily National Centers for Environmental Prediction–National Center for Atmospheric Research (NCEP–NCAR) reanalysis dataset in 6-h intervals with a horizontal resolution of 2.5° × 2.5°. The CMA BTDAT, which consists of 6-h estimates of position, central pressure, and maximum sustained surface wind speed for all named western North Pacific TCs from 1949 to the present (http://www.typhoon.gov.cn/data/detail.php?id=33&type=5), was utilized to evaluate the climatological and persistence variables listed in Table 1. Each variable was evaluated at the beginning ($t = 0$ h) of each 24-h period in the database provided that the system remained over water during the period from $t - 12$ h to $t + 12$ h. The determination as to whether or not these criteria were satisfied was made by using the CMA BTDAT file. A system that remained over land for ≤1 h was designated as an overwater system.

The magnitudes of the maximum sustained surface wind (VMX), latitude (LAT), and longitude (LON) were extracted directly from the BTDAT file. The magnitude of the previous 12-h change in maximum wind speed (DVMX) was evaluated by subtracting VMX at $t = 0$ h from VMX at $t = -12$ h. The u component of the storm

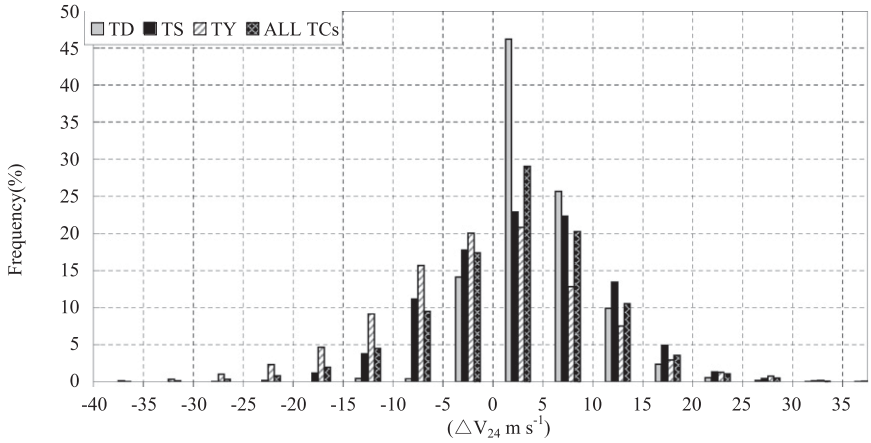

FIG. 1. The frequency distributions of 24-h intensity change (ΔV_{24}) stratified by TC intensity at time $t = 0$ h. The distributions are provided for TDs ($10.8 \leq \text{VMX} \leq 17.1$ m s^{-1}), TSs ($17.2 \leq \text{VMX} \leq 32.6$ m s^{-1}), TYs (VMX ≥ 32.7 m s^{-1}), and all TCs.

motion (USTM) and the storm speed (SPD) were evaluated for the 12-h period centered on the initial ($t = 0$ h) time of each 24-h period. The 24-h change in VMX (ΔV_{24}) was also determined for each 24-h time period by subtracting VMX at $t + 24$ h from VMX at $t = 0$ h, although it is not included in Table 1.

The methodology used to calculate the synoptic oceanic variables is identical to that described in the study of DeMaria and Kaplan (1999, hereafter DK99). Briefly, the sea surface temperature (SST) at each initial TC location was determined from the Reynolds and Smith (1993) gridded 1.0° latitude–longitude weekly analysis available prior to storm passage. The derived SST was then used to compute the empirical maximum potential intensity (MPI). The variable POT listed in Table 1 was then determined by subtracting VMX at $t = 0$ h from the MPI.

The vertical wind shear (SHR) is determined by subtracting the 850- and 200-hPa wind vectors averaged from radius (r) = 200–800 km. The magnitudes of the u component of the 200-hPa wind (U200) and the 200-hPa temperature (T200) are obtained by averaging each of these variables from r = 200–800 km. The relative humidity in the low level of the troposphere (RHLO) is the 850–700-hPa relative humidity averaged from r = 200 to 800 km. The methodology used to compute the 850-hPa relative vorticity (Z850) and the relative eddy flux convergence (REFC) is the same as described in DK99, except that the REFC is evaluated at 200-km intervals and then averaged from r = 200 to 800 km. These variables discussed above are all computed using the NCEP–NCAR reanalysis dataset.

According to the most recent national standard for the level, or grade, of TCs proposed by CMA in 2006, all western North Pacific basin TCs from 1970 to 2007 are divided into three grades. Among the total number of 1214 TCs, there are 212 tropical depressions (TDs, $10.8 \leq \text{VMX} \leq 17.1$ m s^{-1}), 423 tropical storms (TSs, $17.2 \leq \text{VMX} \leq 32.6$ m s^{-1}), and 579 typhoons (TYs, VMX ≥ 32.7 m s^{-1}). These TCs contributed a total of 27 581 cases based on a 6-h observation interval and were subsequently employed in the statistical analyses discussed below.

3. Intensity change distribution

Figure 1 shows the frequency distribution of ΔV_{24}, as a function of the initial ($t = 0$ h) intensity of all 27 581 cases. Slow intensification ($0 \leq \Delta V_{24} < 5$ m s^{-1}) was the most frequently observed 24-h intensity change for any of the intensity classes, indicating TC intensifies during the bulk of its lifetime. Figure 1 shows that a higher fraction of the TS sample than of the TY or TD sample exhibited ΔV_{24} changes exceeding 10 m s^{-1}. Two reasons contribute to this result. First, TSs are further from their MPI than TYs and, thus, have the potential to intensify faster. Second, TSs may intensify more than TDs because of their better initial organization. In contrast, Fig. 1 indicates that TYs are more likely to decay at a fast rate than either TSs or TDs. This is consistent with the higher initial intensities and hence the increased potential of TYs to decay quickly. Although TC intensification occurs for nearly 85% of all TD cases, it occurred in 65% of all TS cases, and 47% of all TY cases. Table 2 summaries the ΔV_{24} distributions shown in Fig. 1. Table 2 shows that the mean change in ΔV_{24} was positive for TDs and TSs, and negative for TYs, indicating that TCs are more likely to intensify with the lower initial intensities. Table 2 also shows that the TY cases had a larger intensity range and standard deviation than either the TS or TD sample. In addition, the TY sample exhibited the largest

TABLE 2. The 24-h intensity change (ΔV_{24}) statistics of the TD, TS, TY, and all TC intensity classes. The number of cases (N), mean, standard deviation (std dev), minimum (min), and maximum (max) ΔV_{24} are also provided.

Intensity class	N	Mean (m s^{-1})	Std dev (m s^{-1})	Min (m s^{-1})	Max (m s^{-1})
TD	8082	3.08	4.97	−15	35
TS	10 810	1.21	8.29	−30	45
TY	8743	−3.45	10.3	−47	35
All TCs	27 581	0.28	8.65	−47	45

decreases in ΔV_{24} of any of the intensity classes. The latter finding may be due, in part, to the comparatively high initial intensities of the TY cases as suggested previously.

One goal of this study is to determine if the large-scale conditions associated with the RI cases were significantly different from those that were present for cases that experienced RD or SC. To be consistent with the previous study in KD03, RI is also defined as the 95th percentile of ΔV_{24} for all of the TC cases used in this study. An RI threshold of 15 m s^{-1} is employed in this study since it is in better agreement with the 95th percentile of the ΔV_{24} distribution of 14.8 m s^{-1}. Similarly, a decrease threshold of 20 m s^{-1} for the 24-h intensity change is employed here to identify the RD cases. The remaining cases belong to the SC cases.

The RI sample employed in this study was composed of 199 TCs compared with the total sample of 1214 TCs. These 199 TCs contributed a total of 561 RI cases, since it was possible for a TC to undergo RI more than once during its lifetime. Table 3 shows the distribution of the total of 561 RI cases as a function of the initial TC intensity. The percentage value in Table 3 obviously shows that the systems that were initially of TS intensity accounted for the largest percentage of RI cases while TYs contributed the next largest percentage and TDs the smallest percentage, and most of them intensified with ΔV_{24} in the range of 20–25 m s^{-1}. Although this result is partly due to variations in the sizes of each of the intensity classes, the likelihood for RI is still greatest for TS and lowest for TD when the number of RI cases in each intensity class is normalized by class sample size. That is, about 2%, 4.29%, and 4.26% of the TD, TS, and TY samples, respectively, underwent RI. Table 3 also indicates that the TY cases composed the largest number of cases in which ΔV_{24} ranged from 20 to 35 m s^{-1} while TS cases composed the largest number of cases with ΔV_{24} exceeding 35 m s^{-1}.

Although the number of 24-h time periods when RI occurred was rather low (not shown), the percentage of systems that underwent RI at least once during their lifetime was comparatively larger. Figure 2 indicates

TABLE 3. The distribution of 24-h intensity change (ΔV_{24}) for the 561 RI cases stratified by intensity class. The numbers of RI cases for each range of ΔV_{24} are also provided. The total number and the percentage of the RI sample total contributed by each of the intensity classes are also presented.

ΔV_{24} (m s^{-1})	TD	TS	TY	All TCs
15–20	27	35	9	71
20–25	47	142	111	300
25–30	15	51	68	134
30–35	1	15	16	32
35–40	2	10	5	17
40–45	0	7	0	7
Total cases	92	260	209	561
Percentage (%)	16.40	46.35	37.25	100

that 11% of all systems that attained TY strength (32.7 ≤ VMX ≤ 41.4 m s^{-1}), 30% of all systems that reached severe TY intensity (41.5 ≤ VMX ≤ 50.9 m s^{-1}), and nearly 70% of all systems that attained supertyphoon strength (VMX ≥ 51 m s^{-1}; the highest percentage) underwent RI at least once during their lifetime. The percentages of systems that underwent RI at least once are all smaller than those of Atlantic systems that underwent RI at least once, as revealed in KD03, indicating that TCs are less likely to experience RI during their lifetime in the western North Pacific basin than in the Atlantic basin due to the different larger-scale conditions. Detailed analysis in section 4 indicates that the upper-level environmental conditions are very different in the two basins. Overall, 18% of all western North Pacific TCs underwent RI.

Figure 3 shows the 24-h tracks and the frequency of the RI cases. Figure 3a indicates that RI generally occurred

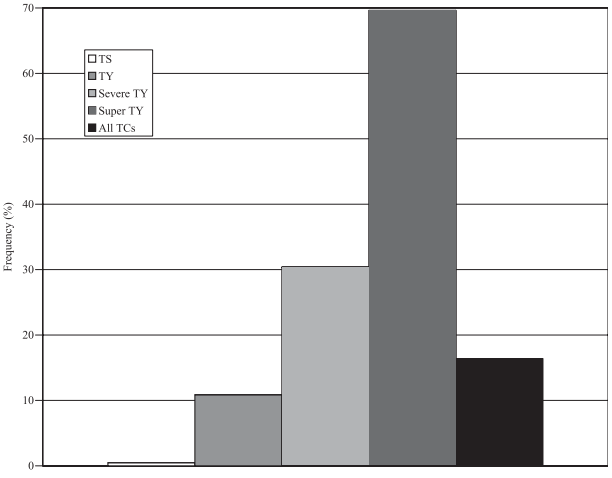

FIG. 2. The percentage of TSs (17.2 ≤ VMX ≤ 32.6 m s^{-1}), TYs (32.7 ≤ VMX ≤ 41.4 m s^{-1}), severe TYs (41.5 ≤ VMX ≤ 50.9 m s^{-1}), supertyphoons (VMX ≥ 51 m s^{-1}), and all TCs that underwent RI at least once during their lifetime as a function of the maximum intensity attained by each system.

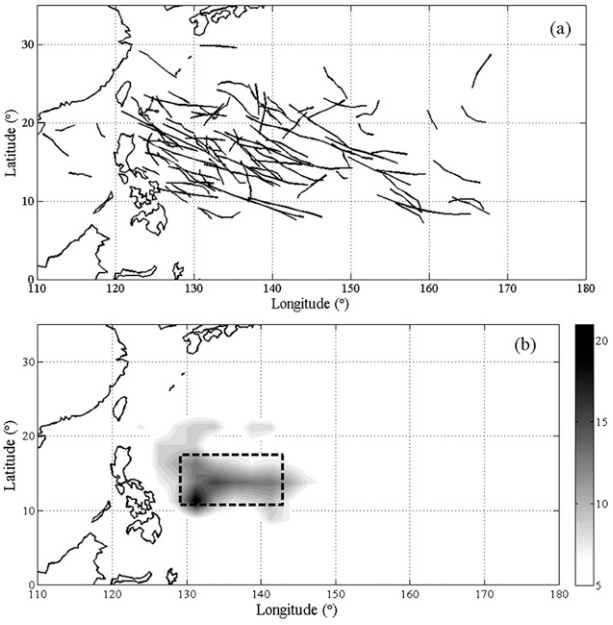

FIG. 3. (a) The 24-h tracks and (b) their frequency for the RI cases. The shading in (b) represents the regions with more than five RI occurrences.

south of 20°N and north of 10°N. Also, these cases mainly moved toward the northwest. From the seasonal distribution of the RI cases (not shown), the majority of the RI cases (nearly 20%) occurred in September and a slightly larger fraction of the RI cases occurred in October (18%) than in July (17%) or August (16%). Figure 3b shows that the RI processes mostly occurred east of the Philippines, as shown by the dashed rectangular region in Fig. 3b.

4. Large-scale conditions associated with RI, SC, and RD cases

a. Comparison of initial conditions

To determine if the initial environmental conditions for the three kinds of samples are significantly different, in this section the larger-scale conditions present at the start of the RI cases are compared to those present at the beginning of the SC or RD cases. Due to the time limitations of the dataset of the weekly 1° × 1° SST, which begins in 1982, the dataset for this comparison only covers the period 1982–2007. A total number of 17 292 cases, consisting of 260 RI samples, 16 660 SC samples, and 372 RD samples during this period, are employed for comparison. Table 4 shows the mean initial values of each of the variables listed in Table 1 for RI, SC, and RD samples. The differences between the mean magnitudes of the RI, SC, and RD samples and their significant levels are also presented in Table 4. The table shows that although the RI and RD cases represent the two extreme stages of TC intensity changes, some large-scale environmental differences between them (D_3 values) are not significant (e.g., Z850 and REFC), indicating that all factors except Z850 and REFC play an important role in modulating TC rapid intensity change. The differences in VMX and SPD between the RI and non-RI cases are also insignificant, which is consistent with the results of the comparison between the RI and non-RI cases in the Atlantic (KD03). But unlike the work in KD03, for the non-RI cases, which include the SC and RD cases, the statistically significant differences exist between the SC and RD samples for VMX and SPD. One

TABLE 4. As in Table 1, but for the mean magnitudes of the initial ($t = 0$ h) climatological and synoptic variables of the RI, SC, and RD cases. The differences between these mean values (D_1 = RI − SC, D_2 = SC − RD, D_3 = RI − RD, and D_4 = RI − non-RI) are also presented.

Variable	Unit	RI	SC	RD	Non-RI	D_1 = RI − SC	D_2 = SC − RD	D_3 = RI − RD	D_4 = RI − non-RI
VMX	m s^{-1}	29.2	27.7	43.6	28.1	1.5[a]	−15.9[c]	−14.3[c]	1.2
LAT	°N	15.9	19.5	23.1	19.5	−3.6[c]	−3.6[c]	−7.2[c]	−3.6[c]
LON	°E	139.0	134.4	124.3	134.2	4.6[c]	10.1[c]	14.7[c]	4.8[c]
SPD	m s^{-1}	4.6	4.7	6.0	4.7	−0.1	−1.4[c]	−1.5[c]	−0.1
DVMX	m s^{-1}	5.0	0.9	−1.7	0.8	4.1[c]	2.6[c]	6.6[c]	4.1[c]
USTM	m s^{-1}	−3.5	−2.0	−1.6	−1.9	−1.5[c]	−0.3	−1.9[c]	−1.5[c]
SST	°C	28.9	28.0	27.3	28.0	0.9[c]	0.7[c]	1.6[c]	0.9[c]
POT	m s^{-1}	50.3	46.4	25.6	46.0	3.9[c]	20.8[c]	24.7[c]	4.4[c]
SHR	m s^{-1}	5.3	8.0	9.2	8.0	−2.7[c]	−1.2[c]	−3.9[c]	−2.7[c]
U200	m s^{-1}	−3.4	−1.4	0.6	−1.4	−2.0[c]	−2.0[c]	−4.0[c]	−2.0[c]
T200	°C	−51.8	−51.2	−50.2	−51.2	−0.5[c]	−1.0[c]	−1.5[c]	−0.6[c]
RHLO	%	78.4	76.9	75.3	76.9	1.5[c]	1.6[c]	3.1[c]	1.6[c]
Z850	10^{-6} s^{-1}	7.8	7.5	7.5	7.5	0.3	0.0	0.3	0.3
REFC	m s^{-1} day^{-1}	−0.9	−1.2	−1.5	−1.2	0.4	0.2	0.6	0.4

[a] The D value difference from the results of a two-sided t test was statistically significant at the 95% level.
[b] The D value difference from the results of a two-sided t test was statistically significant at the 99% level.
[c] The D value difference from the results of a two-sided t test was statistically significant at the 99.9% level.

can further detect the SC (or RD) cases from the non-RI cases based on the magnitudes of the VMX and SPD.

Table 4 indicates that the systems that underwent RI tended to be located farther south and east than the systems that underwent non-RI. These findings are consistent with the climatologically higher SSTs in the southern and eastern portions of the western North Pacific basin (Lin and Zhang 2004), since Table 4 also shows that high SST was characteristics of the RI cases. Also, the RI cases tended to have a more westerly component of motion than did the non-RI cases. Finally, the RI cases were generally intensifying at a faster rate than the non-RI cases during the 12-h period prior to the onset of RI. Although the values of VMX and SPD for all (RI and non-RI) cases are about the same, it can also be seen from Table 4 that the SC cases tended to have a lower initial intensity and a lower speed of motion than do the RD cases. The larger value of SPD for RD cases than RI cases is somewhat surprising in that the previous study (Schade and Emanuel 1999) showed a strong relationship between storm speed and the magnitude of the negative feedback between the ocean and the TC vortex. However, TCs with a fast-moving speed tended to form asymmetrical structures, which inhibited TCs from intensifying (Peng et al. 1999).

The statistically significant differences were also found for SST, RHLO, and POT. Table 4 shows that the RI cases had higher values of SST, RHLO, and POT. The finding that RI occurred in regions with warmer SSTs seems consistent with many previous results (Emanuel 1988; DeMaria and Kaplan 1996; KD03), which found that the higher SSTs would presumably increase the possibility of a TC experiencing large rates of intensification. The higher RHLO values for RI cases are also consistent with the statistical results of KD03 performed in the Atlantic basin. The finding of higher POT values for the RI cases seems reasonable since systems with initial intensities that were further from their MPI would have a greater opportunity to intensify rapidly. Usually, the favorable thermodynamic conditions for SC occurrence fell between those of the RI and RD.

The mean magnitude of SHR is lowest for RI cases and highest for RD cases. The finding of lower values of SHR for the RI cases than for the non-RI cases is consistent with the results of DeMaria and Kaplan (1996). It also agrees with the modeling simulations of Frank and Ritchie (1999), which showed that a TC embedded in an environment with no shear intensified rapidly. Table 4 shows that the RI cases were situated in a more easterly 200-hPa flow and a colder 200-hPa environment. This former finding is reasonable since Fig. 3a also indicates that most RI 24-h tracks are in the northwest or west directions in the prevailing easterly flow. The latter finding is consistent with many observational and theoretical studies (e.g., Zeng et al. 2007; Emanuel 1988). These findings have shown that the outflow temperatures are relatively warm as SSTs are too low to support the normal development of a TC. When a TC intensifies over oceans with high SSTs, the TC vortex itself controls the outflow temperature, which could become colder as a result of the upper-level latent heat release. Usually, the favorable dynamic conditions for SC occurrence fell in the conditions between the RI and RD.

Statistically significant differences were not found between the Z850 and REFC values of the RI and non-RI cases. This finding indicates that Z850 and REFC are not key factors affecting the intensity change of a TC. The latter is consistent with the case studies conducted by Yu and Kwon (2005), who showed that a TC could maintain itself in an environment with or without upper-level eddy momentum forcing.

b. Distribution of large-scale conditions

The results in the above section show that statistically significant differences exist between the mean initial conditions of the RI and non-RI cases for most variables listed in Table 1. In this section, the frequency distributions of these initial conditions are shown for all of the Table 1 variables for which statistically significant differences were found among the three kinds of samples, so that a more comprehensive comparison can be made between the relative likelihood that RI (SC or RD) will occur for any given range of predictor magnitudes.

Figure 4 shows the frequency distributions of the RI and non-RI cases for several of the climatological and persistence variables in Table 1. Figure 4 shows that the frequency distribution of the RI cases is more skewed toward low VMX values than the distribution of RD cases. This seems reasonable since when VMX is high, systems are closer to their MPI and thus have less opportunity to intensify significantly. But relative to the RI cases, the frequency distribution of the SC cases is more skewed toward low VMX values. The distributions of DVMX (Fig. 4) are quite different for the RI and non-RI samples in that the fraction of RI cases that were intensifying at very high rates ($\Delta V_{24} \geq 5$ m s^{-1}) was substantially larger than was observed for the SC and RD cases.

Figure 4 shows notable differences between the distributions of LAT and LON for the RI, SC, and RD samples. Rapid intensification occurs most frequently from 10° to 15°N, and the fraction of RI cases generally decreases with increasing LAT. In contrast, the RD cases occur most frequently from 20° to 25°N and exhibit a much faster poleward decrease. For the SC cases, they occur most frequently at about 15°N. The distributions of

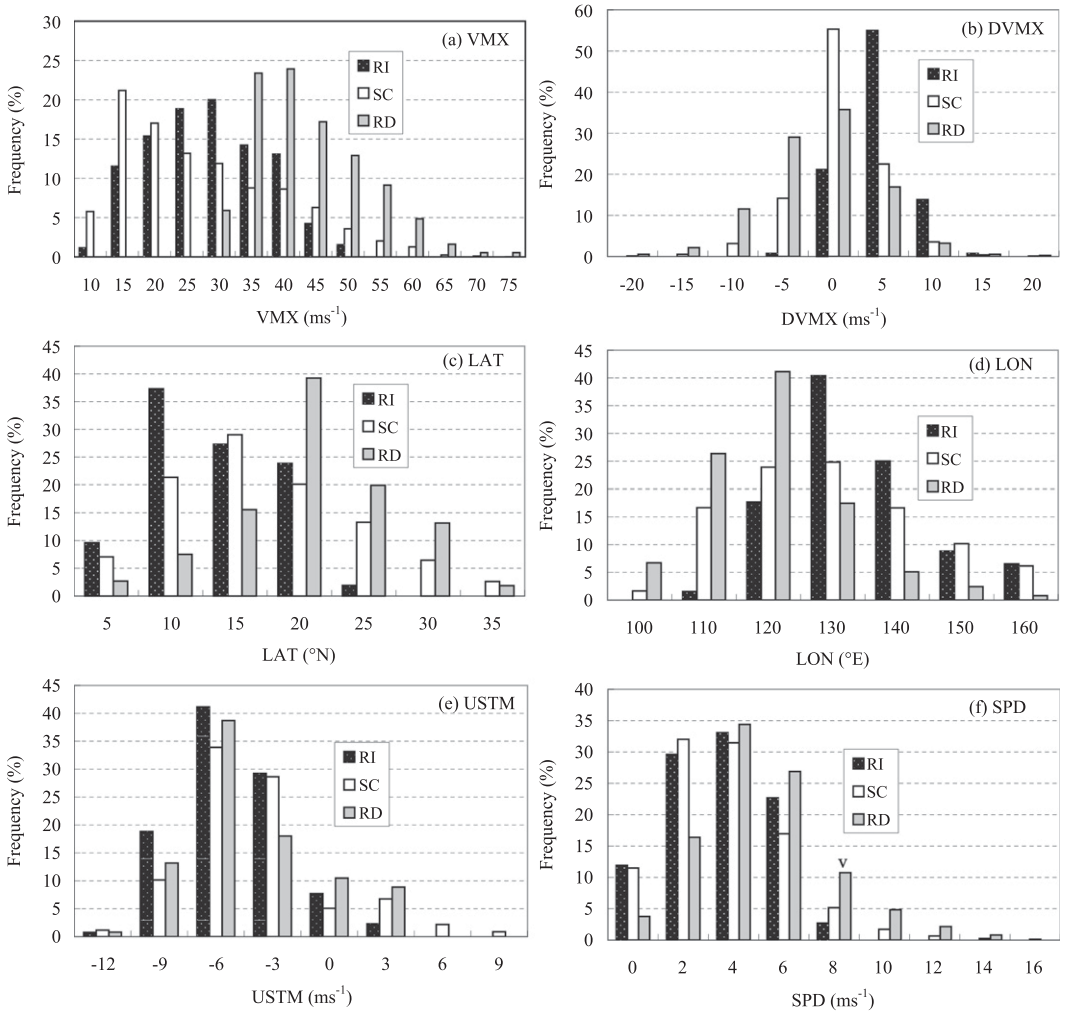

FIG. 4. (a)–(f) Frequency distributions of the climatological and persistence variables for the RI and non-RI samples.

LON values for the RI and RD cases indicate a preference to occur east or west of 130°E for RI and RD cases, respectively. But for SC cases, they can occur at any longitude. The fraction of RI cases generally decreases with increasing LON from 130°E. In contrast, the fraction of RD cases generally decreases with decreasing LON west of 130°E.

Figure 4 shows that a larger fraction of RI cases than non-RI cases were moving westward (USTM < 0), although the distributions of USTM between SC and RD are very similar. Figure 4 also indicates that the distributions of storm speeds (SPD) for the RI and SC cases are quite similar. Although RI was less likely for very slow storm speeds (SPD < 2 m s^{-1}), the majority (70%) of the RI cases occurred for storms moving with SPD from 2 to 8 m s^{-1}, compared with 60% of the RD cases that occurred for storms moving with a larger SPD from 4 to 8 m s^{-1}. This suggests that while slow storm speeds may have a negative impact on TC intensity, other factor such as the deep mixed layers can minimize these effects, as suggested by Schade and Emanuel (1999).

Figure 5 shows the distribution of RI and non-RI cases for the thermodynamic variables. Substantial differences in the SST distributions of the RI and non-RI samples are shown. These are most evident for SSTs above 29°C where the frequency of RI cases was nearly 4 (1.9) times that observed for the RD (SC) samples. Nearly all of the RI cases occurred for SSTs above 28°C. Rapid intensification is also more likely to occur for large values of POT (Fig. 6). This finding is consistent with the aforementioned results that showed that RI was more likely to occur at high SSTs, since a higher SST will yield a larger POT in most of the cases. A notable increase in the fraction of RI cases to non-RI cases was observed for large RHLO values (Fig. 6) with nearly 78% of all RI cases having RHLO exceeding 75%. However, more RD cases than RI cases were observed for RHLO below 75%.

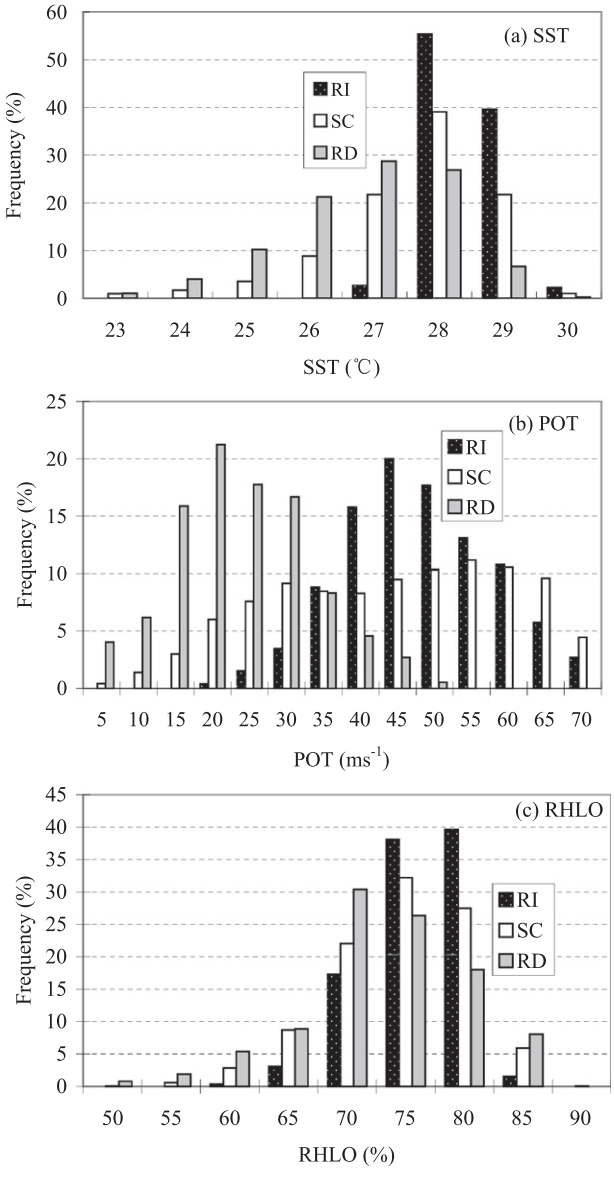

FIG. 5. As in Fig. 4, but for the thermodynamic variables.

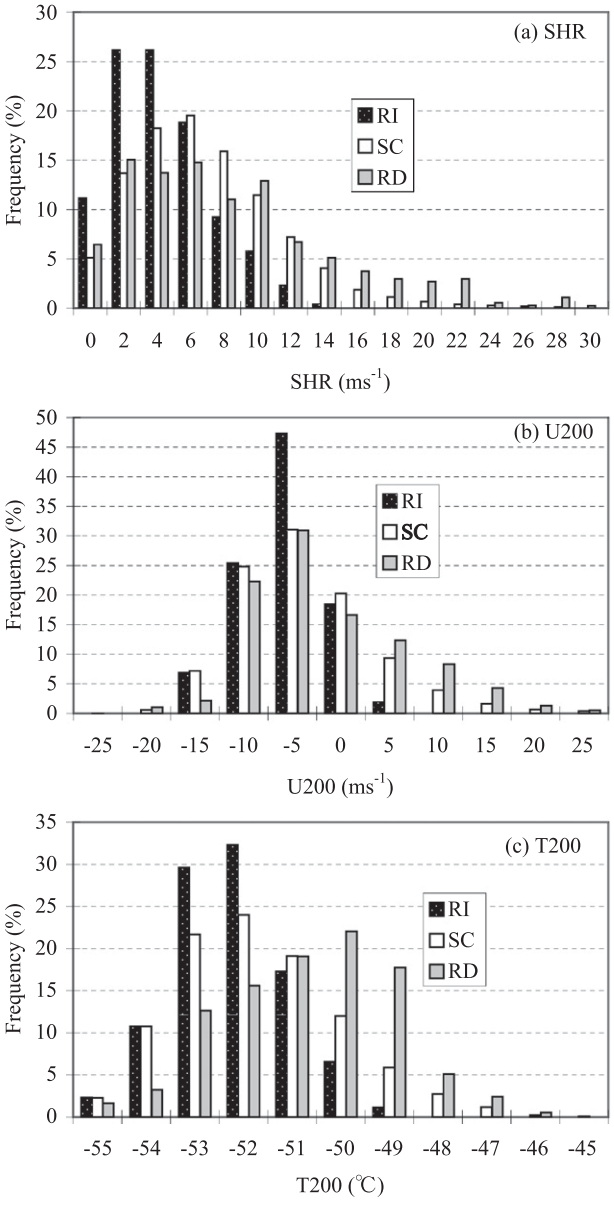

FIG. 6. As in Fig. 4, but for the kinematic variables.

Figure 6 shows the frequency distribution of the RI and non-RI cases for the kinematic variables listed in Table 1. A substantial difference between the distributions of SHR in the RI and non-RI cases is seen. Specifically, 90% of the RI cases occurred when the SHR was less than 8 m s^{-1} compared to 71% of the SC cases and 59% of the RD cases. This suggests that low SHR is an important ingredient for RI. However, RI was also observed for moderate SHR values suggesting that other factors may compensate for increased SHR. The distribution of U200 for the RI cases is skewed toward easterly flow. In addition, the largest fraction of RI cases occurred when U200 was weakly from the east. As for U200, the distribution of T200 for the RI samples is also skewed toward the larger negative values. About 88% of the RI cases occurred for T200 below −50°C compared to only 43% of the RD cases. As with the results of Emanuel (1988), who showed that very cold upper-level temperatures may have increased the environmental sustained maximum intensity of a TC, this finding suggests that systems with cold upper-level outflow temperature may have more opportunity to intensify significantly.

5. Estimating the probability of RI

In this section, estimates of the probability of RI are obtained using the same method developed by Kaplan

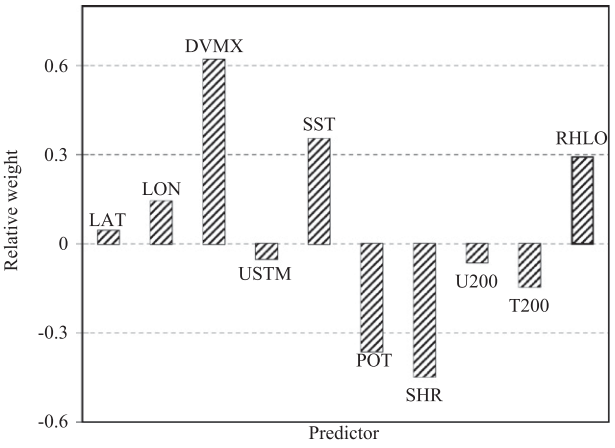

FIG. 7. The relative weights of the western North Pacific basinBasin RI predictors.

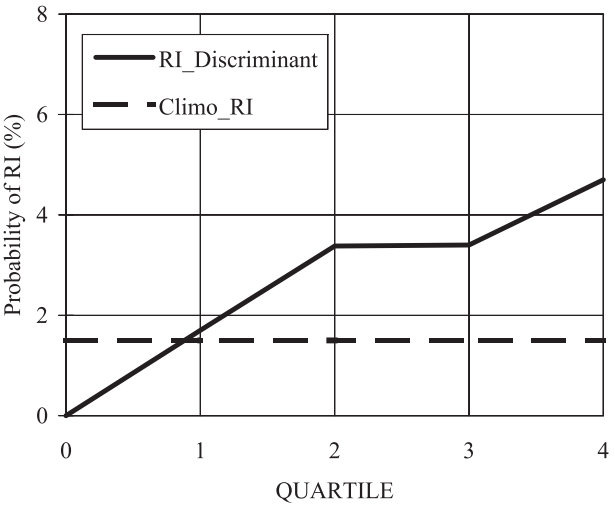

FIG. 8. The probability of RI for the western North Pacific basin for the discriminant RII. The climatological RI probabilities (dash lines) are also shown.

et al. (2010), which is a revised predictor RI index based on the original version described in KD03. The predictors selected for use in the western North Pacific basin RII include those for which it had been shown that statistically significant differences existed at the 99.9% level between the mean values of the RI and non-RI samples based upon a two-sided *t* test listed in Table 1. Thus, 10 predictors (LAT, LON, DVMX, USTM, SST, POT, SHR, U200, T200, and RHLO) are employed in setting up the western North Pacific basin RII.

As described in the study of Kaplan et al. (2010), two methods are used to estimate the probability of RI. The first one is the scaled version, which uses the scaled magnitudes of the predictors to determine the likelihood of RI. After the scaled magnitude of each of the RI predictors (S_{P_a}) is obtained, the total scaled value of each forecast case (RI and non-RI cases) R_s is obtained by summing these S_P values [see Eq. (1) in Kaplan et al. (2010)]. Because the scaled method does not account for the relative importance of each predictor to RI, the second method is developed to determine the likelihood of RI. The weights (W_n) of each of the RI predictors are first obtained by performing a linear discriminant analysis, and then multiplied by the S_P values. Figure 7 shows the W_n of the 10 RI predictors. It can be seen that the predictor DVMX has the largest weight value, indicating its great effect on RI occurrence. Besides DVMX, the kinematic predictor SHR has a slightly larger weight than the weights of the thermodynamic predictors SST, POT, and RHLO, indicating their very important impacts on RI occurrence compared to other factors. It can also be seen that the predictors LON, USTM, U200, and T200 have the smaller weight values, suggesting their negligible impacts on RI occurrence. The discriminant value of each forecast case R_d is finally obtained by summing the weighted S_P values of each of the RI predictors. In this study, we use the same two methods (scaled version and discriminant version) to estimate the likelihood of RI after the R_s or R_d values of each of the 24-h forecast cases are placed into quartiles.

Figure 8 shows the probability of RI for "discriminant" versions of the RII. The probability obtained for the scaled version of the RII (not shown) is a little lower than that in Fig. 8. It can be seen that the RI probability is lowest (highest) for the first (fourth) quartile with the lowest (highest) R_d values. The climatological probability of RI is also shown to provide a measure of the likelihood that RI will occur for any given 24-h forecast period. It is computed by dividing the number of RI cases by the total number of RI and non-RI cases in the full set of 1982–2007 developmental samples. It can be seen that the RI probability for the second quartile is at least a factor of 2 greater than climatological while the probability computed for the fourth quartile is even greater.

The skill of the RII forecasts made for the 1982–2007 developmental sample is assessed by computing the Brier score (BS; Wilks 2006) of those forecasts and comparing it to the BS of forecasts computed based on the climatological probability of RI. The skill of the scaled or discriminant RII is then evaluated using the Brier skill score (BSS; Wilks 2006):

$$\mathrm{BSS} = \left(1 - \frac{\mathrm{BSM}}{\mathrm{BSC}}\right) \times 100,$$

where BSM is the Brier score of the RII forecasts and BSC is the Brier score of the climatological forecasts. Thus, positive values of BSS indicate that the RII exhibited skill relative to climatology while negative

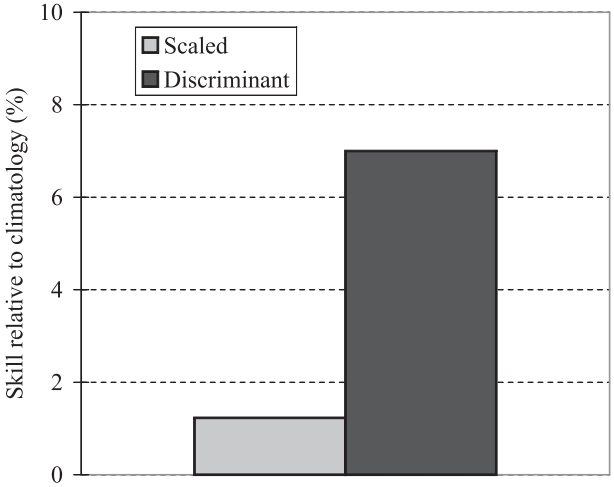

FIG. 9. The skill of the scaled and discriminant versions of the western North Pacific basin RII relative to forecasts based on climatology for the 1982–2007 developmental sample.

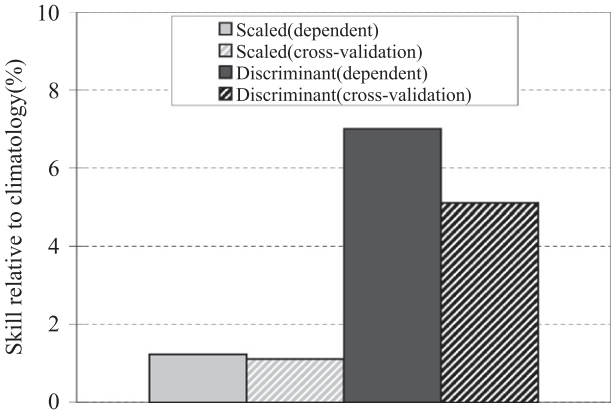

FIG. 10. The skill levels of the western North Pacific basin RII for the 1982–2007 dependent and independent cross-validation forecasts. The skill is depicted for both the scaled and discriminant versions of the RII.

values indicate that the RII was not skillful. Figure 9 depicts the skill of the RII for both scaled and discriminant versions of the RII for the 1982–2007 developmental data sample. It can be seen that both are skillful and that the discriminant version is much more skillful than the scaled version. Kaplan et al. (2010) yielded similar results for their Atlantic basin RII.

6. Verification of the RII for independent samples

The results from the above section show that the RII is skillful relative to forecasts made based on climatology for the 1982–2007 developmental sample. In this section, the method of cross validation (Wilks 2006) is employed to verify the RII for an independent sample to better assess its potential performance. To accomplish this, the storms from each of the individual years that composed the 26-yr developmental sample (1982–2007) are excluded and the RII is rederived using only cases from the remaining 25-yr sample. The RII that is derived using data from the 25 yr of developmental data is then run on the cases from the excluded year. This procedure is repeated for each of the individual years that composed the 26-yr western North Pacific basin samples and the results are tabulated to obtain the skill of the RII for the period 1982–2007.

Figure 10 shows the skill of the scaled and discriminant versions of the RII utilizing the cross-validation technique described above for the western North Pacific basin. The skill of the RII for the developmental sample (Fig. 9) is also provided. It can be seen that the RII has skill in the western North Pacific basin. However, as expected, the skill is somewhat less than that previously obtained for the developmental sample. The decrease in skill is smaller for the scaled version of the RII compared to the discriminant version. This finding is reasonable since the techniques for computing the values of R_s and R_d are different; the latter changes more significantly with the number of developmental sample changing.

The aforementioned probabilistic verification showed that the probability obtained using the RII is generally skillful compared to that based on climatology. In the section below, the capability of the RII to forecast episodes of RI using a more deterministic approach is evaluated. Prior to performing the deterministic approach, a single probability threshold for forecasting whether or not RI will occur over the succeeding 24 h should be determined. As described in Wilks (2006), the value of the discriminant function that matches the climatological probability of false detection (POFD, the ratio of the number of times that an event is forecast to occur but does not, divided by the total number of times that an event does not occur; also known as the false alarm rate) of the dependent sample is used to determine whether to assign a case to the RI or non-RI group. The climatological POFD can be approximated by the climatological probability of RI divided by one plus the climatological probability of RI. The above quartile methodology is repeatedly employed to estimate the POFD between each of the four quartiles. Finally, the probability of an RI cutoff threshold for the western North Pacific basin is obtained when the POFD computed from the developmental sample matching that of climatology.

The samples in the period 1986–2007 are used to verify the skill of the RII for independent samples. To do this, the 1986–2006 RI cutoff threshold is used to make forecasts of RI for the independent 2007 sample, while

the 1986–2005 and 2007 RI cutoff thresholds are used to make a forecast for the independent 2006 sample. The procedure is repeated for each of the individual years that compose the 22-yr (1986–2007) western North Pacific basin samples. RI is forecast if the probability of RI equals or exceeds the probability of the RI cutoff threshold.

The three metrics used to evaluate the skill of the RI forecast are the probability of detection (POD), the false alarm ration (FAR), and the Peirce skill score (PSS). The POD (Wilks 2006) is the percentage of the RI cases that are correctly identified. The FAR is the number of times that RI is forecasted but does not occur divided by the total number of times RI is forecast. The PSS is used to evaluate the overall skill of contingency-type forecasts and is particularly helpful for evaluating forecasts of such rare events as RI (Wilks 2006). The PSS is equivalent to POD − POFD and is 1 for a perfect forecast, 0 for random or constant forecasts, and negative for even worse forecasts than random forecasts. The verification of the deterministic RI forecast for the western North Pacific basin for the 1986–2007 tropical cyclone seasons showed that the average POD of the RII is nearly 70%. The averaged PSS for the RII is positive (about 0.1), indicating that the RII has skill for the independent western North Pacific sample.

7. Conclusions

As defined in this study, RI was determined as being approximately the 95th percentile of all 24-h overwater intensity changes of western North Pacific basin TCs that developed from 1970 to 2007. This equaled a maximum sustained surface wind speed increase of 15 m s^{-1} over a 24-h period. Over the western North Pacific basin, TCs were intensifying for most of their lifetimes. Of all 27 581 data samples, 85%, 65%, and 47%, respectively, of all TDs, TSs, and TYs intensify. Of the 1214 tropical cyclones that composed the 1970–2007 samples, 18%, 70%, 30%, and 10%, respectively, of all tropical cyclones, supertyphoons, severe typhoons, and typhoons underwent RI at least once during their lifetime.

The definition for RD of a 24-h maximum sustained surface wind speed decrease of ≥20 m s^{-1} is also used in the current study. Limited by the dataset, all 17 292 cases including 260 RI cases, 372 RD cases, and 16 660 SC (slow change in intensity) cases during the period 1982–2007 were used to analysis the large-scale conditions associated with RI and non-RI (including the SC and RD) cases. The results showed that the RI cases tended to occur farther south and east than the non-RI cases. In addition, the RI cases had a more westerly component of motion and were intensifying more during the preceding 12 h than the non-RI cases. Although the differences in the storm initial intensity and the speed of motion between the RI and non-RI were not significant, these differences were very significant between the SC and RD cases. The SC cases tended to have a lower initial intensity and a lower speed of motion than the RD cases.

The RI cases were farther from their maximum potential intensity and developed in regions of warmer water and higher lower-tropospheric relative humidity than the non-RI cases. Also, the RI cases were in regions of lower vertical shear and more easterly upper-tropospheric flow than the non-RI cases. Usually, the favorable conditions for SC occurrence fell in the conditions between the RI and RD.

A rapid intensity index (RII) was developed for the western North Pacific basin. The RII employed large-scale predictors that were statistically significant at the 99.9% level using a two-sided t test to estimate the probability of RI over the succeeding 24 h. The probabilistic verification based upon the cross validation from 1982 to 2007 tropical cyclone seasons showed that the RII was skillful relative to climatology for the western North Pacific basin. Moreover, even if utilized in the scaled manner for the 1986–2007 tropical cyclone seasons, the RII performed well in terms of the high POD and the positive PSS. However, some other large-scale and more detailed inner-core information should be considered in the RII to further improve the skill of this index in the near future.

Acknowledgments. This study is supported by the National Science Foundation of China (40905020, 40830958), the National Basic Research Program of China (2009CB421502), the Fundamental Research Funds for the Central Universities (1117020704), the Special Fund for Meteorology Research in the Public Interest (GYHY201006007), and the Funds for the Priority Academic Program Development of Jiangsu Higher Education Institutions (PAPD).

REFERENCES

Bender, M. A., and I. Ginis, 2000: Real-case simulations of hurricane–ocean interaction using a high-resolution coupled model: Effects on hurricane intensity. *Mon. Wea. Rev.,* **128,** 917–943.

Black, P. G., 1983: Ocean temperature changes induced by tropical cyclones. Ph.D. dissertation, The Pennsylvania State University, 278 pp. [Available from The Pennsylvania State University, University Park, PA 16802.]

Bosart, L. F., C. S. Velden, W. E. Bracken, J. Molinari, and P. G. Black, 2000: Environmental influences on the rapid intensification of Hurricane Opal (1995) over the Gulf of Mexico. *Mon. Wea. Rev.,* **128,** 322–352.

Byers, H. R., 1944: *General Meteorology*. McGraw-Hill, 645 pp.

Chan, C. L., Y. H. Duan, and L. K. Shay, 2001: Tropical cyclone intensity change from a simple ocean–atmosphere coupled model. *J. Atmos. Sci.,* **58,** 154–172.

Cione, I. J., and E. W. Uhlhorn, 2003: Sea surface temperature variability in hurricanes: Implications with respect to intensity change. *Mon. Wea. Rev.,* **131,** 1783–1796.

DeMaria, M., and J. Kaplan, 1996: The effect of vertical shear on tropical cyclone intensity change. *J. Atmos. Sci.,* **53,** 2076–2087.

——, and ——, 1999: An updated statistical hurricane intensity prediction scheme for the Atlantic and eastern North Pacific basins. *Wea. Forecasting,* **14,** 326–337.

——, J. A. Knaff, and C. Sampson, 2007: Evaluation of long-term trends in tropical cyclone intensity forecasts. *Meteor. Atmos. Phys.,* **97,** 19–28.

Eastin, M., W. M. Gray, and P. G. Black, 2005a: Buoyancy of convective vertical motions in the inner core of intense hurricanes. Part I: General statistics. *Mon. Wea. Rev.,* **133,** 188–208.

——, ——, and ——, 2005b: Buoyancy of convective vertical motions in the inner core of intense hurricanes. Part II: Case studies. *Mon. Wea. Rev.,* **133,** 209–227.

Elsberry, R., T. D. B. Lambert, and M. A. Boothe, 2007: Accuracy of Atlantic and eastern North Pacific tropical cyclone intensity forecast guidance. *Wea. Forecasting,* **22,** 747–762.

Emanuel, K. A., 1988: The maximum intensity of hurricanes. *J. Atmos. Sci.,* **45,** 1143–1155.

——, 2000: Thermodynamic control of hurricane intensity. *Nature,* **401,** 665–669.

Frank, W. M., and E. A. Ritchie, 1999: Effects of environmental flow upon tropical cyclone structure. *Mon. Wea. Rev.,* **127,** 2044–2061.

——, and ——, 2001: Effects of vertical wind shear on the intensity and structure of numerically simulated hurricanes. *Mon. Wea. Rev.,* **129,** 2249–2269.

Gray, W. M., 1968: Global view of the original of tropical disturbances and storms. *Mon. Wea. Rev.,* **96,** 669–700.

Hanley, D., J. Molinari, and D. Keyser, 2001: A composite study of the interactions between tropical cyclones and upper-tropospheric troughs. *Mon. Wea. Rev.,* **129,** 2570–2584.

Holliday, C. R., and A. H. Thompson, 1979: Climatological characteristics of rapidly intensification typhoons. *Mon. Wea. Rev.,* **107,** 1022–1034.

Hong, X., S. W. Chang, S. Raman, L. K. Shay, and R. Hodur, 2000: The interaction between Hurricane Opal (1995) and a warm core ring in the Gulf of Mexico. *Mon. Wea. Rev.,* **128,** 1347–1365.

Kaplan, J., and M. DeMaria, 2003: Large-scale characteristics of rapidly intensifying tropical cyclones in the North Atlantic basin. *Wea. Forecasting,* **18,** 1093–1108.

——, ——, and J. A. Knaff, 2010: A revised tropical cyclone rapid intensification index for the Atlantic and eastern North Pacific basins. *Wea. Forecasting,* **25,** 220–241.

Kossin, J., and W. H. Schubert, 2001: Mesovortices, polygonal flow patterns, and rapid pressure falls in hurricane-like vortices. *J. Atmos. Sci.,* **58,** 1079–1090.

Lin, H. J., and Y. C. Zhang, 2004: Climatic features of the tropical cyclone influencing China and its relationship with the sea surface temperature in the Pacific Ocean (in Chinese). *J. Trop. Meteor.,* **20,** 218–224.

Lowag, A., M. L. Black, and M. D. Eastin, 2008: Structural and intensity changes of Hurricane Bret (1999). Part I: Environmental influences. *Mon. Wea. Rev.,* **136,** 4320–4333.

Mainelli, M., M. DeMaria, L. K. Shay, and G. Goni, 2008: Application of oceanic heat content estimation to operational forecasting of recent Atlantic category 5 hurricanes. *Wea. Forecasting,* **23,** 3–16.

Malkus, J. S., and H. Riehl, 1960: On the dynamics and energy transformations in steady-state hurricanes. *Tellus,* **12,** 1–10.

Merrill, R. T., 1988: Environmental influences on hurricane intensification. *J. Atmos. Sci.,* **45,** 1678–1687.

Miller, B. L., 1958: On the maximum intensity of hurricanes. *J. Meteor.,* **15,** 184–195.

Molinari, J., and D. Vollaro, 1990: External influences on hurricane intensity. Part II: Vertical structure and response of the hurricane vortex. *J. Atmos. Sci.,* **47,** 1902–1918.

Montgomery, M. T., and R. J. Kallenbach, 1997: A theory for vortex Rossby waves and its application to spiral bands and intensity changes in hurricanes. *Quart. J. Roy. Meteor. Soc.,* **123,** 435–465.

Palmén, E., 1948: On the formation and structure of tropical hurricanes. *Geophysica,* **3,** 26–38.

Peng, M. S., B. F. Jeng, and R. T. Williams, 1999: A numerical study on tropical cyclone intensification. Part I: Beta effect and mean flow effect. *J. Atmos. Sci.,* **56,** 1404–1423.

Pfeffer, R. L., 1958: Concerning the mechanics of hurricanes. *J. Meteor.,* **15,** 113–120.

——, and M. Challa, 1981: A numerical study of the role of eddy fluxes of momentum in the development of Atlantic hurricanes. *J. Atmos. Sci.,* **38,** 2393–2398.

Reynolds, R. W., and T. M. Smith, 1993: An improved real-time global sea surface temperature analysis. *J. Climate,* **6,** 114–119.

Schade, L. R., and K. A. Emanuel, 1999: The ocean's effect on the intensity of tropical cyclones: Results from a simple coupled atmosphere–ocean model. *J. Atmos. Sci.,* **56,** 642–651.

Shay, L. K., G. J. Goni, and P. G. Black, 2000: Effects of a warm oceanic feature on Hurricane Opal. *Mon. Wea. Rev.,* **128,** 1366–1383.

Sitkowski, M., and G. M. Barnes, 2009: Low-level thermodynamic, kinematic, and reflectivity fields of Hurricane Guillermo (1997) during rapid intensification. *Mon. Wea. Rev.,* **137,** 645–663.

Sutyrin, G. G., and A. P. Khain, 1979: Interaction of the ocean and the atmosphere in the area of moving tropical cyclone. *Dokl. Akad. Nauk. SSR,* **249,** 467–470.

Ventham, J. D., and B. Wang, 2007: Large-scale flow patterns and their influence on the intensification rates of western North Pacific tropical storms. *Mon. Wea. Rev.,* **135,** 1110–1127.

Wang, B., and X. Zhou, 2008: Climate variation and prediction of rapid intensification in tropical cyclones in the western North Pacific. *Meteor. Atmos. Phys.,* **99,** 1–16.

Wilks, D. S., 2006: *Statistical Methods in the Atmospheric Sciences*. 2nd ed. Academic Press, 627 pp.

Willoughby, H. E., J. A. Clos, and M. G. Shoreibah, 1982: Concentric eyewalls, secondary wind maxima, and the evolution of the hurricane vortex. *J. Atmos. Sci.,* **39,** 395–411.

Yu, H., and H. J. Kwon, 2005: Effect of TC–trough interaction on the intensity change of two typhoons. *Wea. Forecasting,* **20,** 199–211.

Yuan, T., and H. Jiang, 2010: Forecasting rapid intensification of tropical cyclones in the western North Pacific using TRMM/TMI 37 GHz microwave signal. *Extended Abstracts, 65th Interdepartmental Hurricane Conference (IHC),* Miami, FL, Office of the Federal Coordinator for Meteorological Services and Supporting Research (OFCM). [Available online at http://www.ofcm.gov/ihc11/linking_file_ihc11.htm.]

Zeng, Z., Y. Wang, and C. C. Wu, 2007: Environmental dynamical control of tropical cyclone intensity—An observational study. *Mon. Wea. Rev.,* **135,** 38–60.